Discussion

The present analysis has established the complete structure of *anti*-7-norbornenyl *p*-bromobenzoate. The interesting part of the molecule is the norbornene nucleus. The carbon–carbon single bonds are all of normal length, the mean distance being 1·54 Å; the C=C bond length is 1·34 Å. The valency angles are given in Table 3 and are illustrated in Fig. 3; the norbornene nucleus has symmetry *m* within experimental error. All the angles are less than the tetrahedral value, indicating considerable strain in the skeleton; the angles at the double bond are only 107°. The bridgehead angle is 95·6°.

The corresponding features in the tricyclo-octane nucleus (Macdonald & Trotter, 1965) are included in Fig. 3 for comparison. The skeletons are obviously very similar. The angles between the various planes in the norbornenyl nucleus, illustrated in Fig. 3, are given in Table 4, $A\widehat{\ }B=111°$, $A\widehat{\ }D=123°$, $B\widehat{\ }D=126°$, identical with the corresponding angles in the tricyclo-octyl skeleton. The C(1)...C(4) distances are equal. The bridgehead angles (97° in the tricyclo-octane nucleus, 96° in the norbornene nucleus) are identical within experimental error.

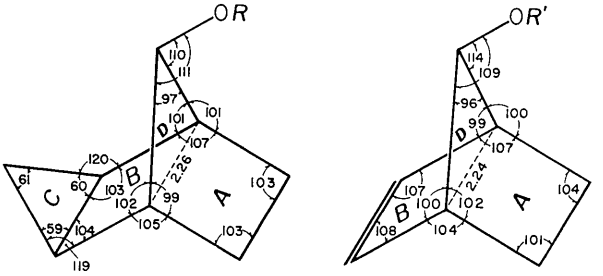

Fig. 3. Bond angles in the tricyclo-octane and norbornene nuclei.

The rate of solvolysis of the *p*-bromobenzenesulphonyl derivative of *anti*-7-norbornenol (III, $R=p$-bromobenzenesulphonyl) is about 10^{11} faster than that of the corresponding derivative of *anti*-8-tricyclo-octanol (V, $R=p$-bromobenzenesulphonyl), and since the bridgehead angles are the same in the two skeletons, variation in bridgehead angle cannot be the explanation for variation in solvolysis rate.

The bond distances and valency angles in the *p*-bromobenzoyl group are all normal; Br–C=1·90 Å, mean C_{ar}–C_{ar}=1·39 Å, C_{ar}–$C_{carboxyl}$=1·44 Å, C=O=1·20Å, C–OR=1·34 Å, O–R=1·44 Å, mean angle at C_{ar}=120°, C–C=O=123°, C–C–O=114°, O=C–O=123°, C–O–C=117°. The intermolecular distances (Table 5) all correspond to van der Waals interactions.

The authors are indebted to Dr R. E. Pincock and Mrs J. I. Wells for suggesting the problem and for supplying the crystal sample; to Dr F. R. Ahmed and Dr G. A. Mair for making available their IBM 1620 programs, and to the staff of the U.B.C. Computing Centre for assistance; to the National Research Council of Canada and to the Committee on Research, Faculty of Graduate Studies, University of British Columbia, for financial support, and to the Department of Scientific and Industrial Research, United Kingdom, for the award of a research studentship (to A.C.M.).

References

FURNAS, T. C. (1957). *Single Crystal Orienter Instruction Manual.* Milwaukee: General Electric Company.

International Tables for X-Ray Crystallography (1962). Vol. III. Birmingham: Kynoch Press.

MACDONALD, A. C. & TROTTER, J. (1965). *Acta Cryst.* **18**, 243.

SCHLEYER, P. R. & NICHOLAS, R. D. (1961). *J. Amer. Chem. Soc.* **83**, 182.

Acta Cryst. (1965). **19**, 463

On the Cementite Structure

BY E. J. FASISKA AND G. A. JEFFREY

The E. C. Bain Fundamental Research Laboratory, United States Steel Corporation, and The Crystallography Laboratory, The University of Pittsburgh, Pittsburgh, Pa. U.S.A.

(*Received* 25 *September* 1964 *and in revised form* 7 *December* 1964)

The preparation of single crystals of $(Fe_{2\cdot7}Mn_{0\cdot3})C$ has permitted a complete three-dimensional anisotropic refinement of the cementite structure with this composition. The atomic coordinates of the metal and carbon atoms have been determined to an estimated standard deviation of 0·001 Å and 0·01 Å respectively.

The structure can be rationally described in terms of a pleated-layer hexagonal arrangement of the iron atoms and as such is related to the structures of ε-iron and the ε-carbide.

Introduction

Cementite, Fe_3C, has been the subject of a large number of publications bearing upon its phase and structural relationships to iron and the other iron carbides, of which recent examples are those of Andrews (1963, 1964). This and closely related structures also occur in certain binary compounds especially borides, of the

seventh and eighth group metals (Aronsson & Rundquist, 1962). Hitherto, the definitive structure analysis was that of Lipson & Petch (1940) in which the seven atomic positional parameters were deduced from visual intensity measurements of twenty-three powder lines, of which four were unresolved. It is a remarkable tribute to the ingenuity of these workers and the power of the Fourier analysis methods that they used that, as we will show, their iron positions are probably correct to within 0·03 Å and their carbon positions to 0·12 Å. Subsequent electron diffraction (Gardin, 1962), and neutron diffraction (Meinhardt & Krisement, 1962; Lyashchenko & Sorokin, 1963) made no further contribution to the crystal structural data. The difficulty, a familiar one in crystallography, was that no single crystals of cementite could be obtained. The observation (Shigetaka, 1930) that addition of manganese would facilitate the growth of crystals prompted experiments which gave single crystals suitable for X-ray structure analysis containing 10% manganese. We have therefore carried out a complete three-dimensional analysis using modern techniques on one of these crystals. We have also described the cementite structure in a way which we believe permits a simpler discussion of the relationship to other iron phases, particularly ε-iron and the ε-carbide.

Experimental

The crystals were grown in a vertical Bridgman furnace under vacuum from a 9% Mn, 91% Fe alloy held in a graphite crucible at 1143 °C for 45 hours and then air cooled. A wet chemical analysis of the crystals and matrix in which they appear showed a mean manganese content of 8%. An analysis by scanning with a 2μ beam electron probe microanalyzer gave $10{\cdot}0 \pm 0{\cdot}5\%$ manganese for the crystals and $5{\cdot}5 \pm 0{\cdot}5\%$ manganese for the matrix.

Needles elongated about all three principal axes were obtained, and one about [*a*] was selected by reason of its shape and dimensions. It was 1 mm long with a distorted hexagonal cross section which was constant over its entire length with a mean diameter of 0·1 mm.

The crystal was first investigated X-ray-photographically to establish that there were no anomalies in the diffraction spectra as compared with an undisordered and unstrained crystal with the structure described by the Lipson & Petch data. For this purpose a set of equi-inclination Weissenberg photographs were taken which subsequently also proved useful as a guide in the measurement of the counter data. The intensities were measured with zirconium-filtered Mo $K\alpha$ radiation, using a General Electric Single Crystal Orienter and XRD-3 diffractometer with a proportional counter. The visual alignment of the crystal on the orienter was greatly simplified by attaching the chuck of an 800 r.p.m. electric drill to the φ angle control knob. The setting angles for the orienter and the 2θ angles were computed on an IBM 1620 with Shiono's (1962) program, from the known unit-cell dimensions. For most measurements, a further small adjustment was necessary to maximize the intensity. The reflections were $\theta/2\theta$ scanned at 0·2° of 2θ per minute so as to record the backgrounds and α_1 and α_2 peaks on a strip chart recorder. The 002 reflection was used as a standard which was measured by means of a planimeter on the recorder traces. The background was estimated on the assumption that it varied linearly across the peak. The reflections which were too weak to record in this manner were measured by counting on $K\alpha_1$ for one minute and normalizing against a similar count on the $K\alpha_1$ peak for 002. Altogether 1000 independent reflections were sought, and 780 were measured. The total time for these measurements was about 250 hours.

The intensities were corrected for absorption by a FORTRAN program by Craven (1963) on a Control Data Corporation G-20 Computer. These corrections were compared against those for a cylindrical crystal of similar dimensions with Table 5.3.5 of *International Tables for X-ray Crystallography* (1959) .The use of the much simpler cylindrical approximation would have introduced errors of intensities averaging about twenty five per cent of the corrected intensities. The Lorentz and polarization factors were applied by means of an IBM 1620 program (Dutta, 1964).

The crystal data

The unit-cell dimensions of both $(Fe_{2\cdot7}Mn_{0\cdot3})C$ and Fe_3C were measured from powder photographs, with the use of the Cohen extrapolation technique, and are given in Table 1. The $(Fe_{2\cdot7}Mn_{0\cdot3})C$ powder was obtained by crushing several crystals. The Fe_3C was extracted from a 1·32 wt.% C-Fe alloy which had been hot rolled to 0·1 inch, reheated to 788 °C and furnace cooled producing large partially spheroidized particles. Our lattice parameter values for Fe_3C agreed with those of Lipson & Petch (1940) within $2\frac{1}{2}$ of the estimated standard deviations of 0·01%.

Table 1. *Lattice parameters of some cementite structures*

	a	*b*	*c*	Volume (Å³)
$(Fe_{2\cdot7}Mn_{0\cdot3})C$	5·0598	6·7462	4·5074	153·86
Fe_3C	5·0896	6·7443	4·5248	155·32
e.s.d.	0·0005 Å	0·0007 Å	0·0005 Å	
Fe_3C	5·0890	6·7433	4·5235	155·23*
Mn_3C	5·080	6·772	4·530	155·84†

* Lipson & Petch (1940). † Kuo & Persson (1954).

There is a small, but significant, one per cent contraction in cell volume as the Mn atoms replace Fe, but this is not isotropic; in fact, there is a small expansion in the *b*-axis dimension. This can be compared with the Mn_3C dimensions, also given in Table 1. The *a* and *c* parameters are probably not significantly different from those of Fe_3C, but the *b* parameter is increased. The overall contraction of the lattice at the

10% manganese composition is in contrast to the small but uniform expansion of the α-iron, γ-iron, and wustite lattices by the addition of manganese (Pearson, 1958). This appears to be a particular characteristic of the cementite structure, which suggests that there may be an ordering of the manganese atoms in some composition ranges. Such ordering could not, of course, be observed from X-ray study.

The space group of the cementite structure is *Pnma* (No. 62) with iron atoms in 8-fold general positions (*d*) and 4-fold positions (*c*), and carbon atoms in 4-fold positions (*c*). The calculated densities for $(Fe_{2\cdot7}Mn_{0\cdot3})C$ and Fe_3C are 7·739 and 7·678 g.cm^{-3} respectively.

The refinement calculations

The initial parameters used for the structure factor calculations were those of Lipson & Petch (1940) for Fe_3C and are given in Table 1 in Å. A Wilson plot on the three-dimensional data gave a scaling factor and overall isotropic temperature factor. A least-squares calculation was run initially on the IBM 7070 computer with Carpenter's (1963) program and finally on the IBM 7090 computer with the Busing, Martin & Levy (1962) program, in the anisotropic mode. Initially all the 770 observed reflections were used. Of these, six strong low-order reflections (031, 060, 210, 220, 230, 430) showed exceptionally poor agreement, being up to 30% lower than the calculated values. They were therefore omitted from the later least-squares calculations, (as were the *h*00 reflections which were not measured from the crystal mounted about the *a* axis).

During the refinement cycles, it was observed that although the error of fit was decreasing, the agreement index was increasing. An analysis of the distribution of the ΔF's revealed that the high agreement index was located in those weak reflections whose intensities were measured by the peak-height method. These were also omitted from the calculation, leaving the 550 reflections all of which had been measured by integrated planimetry. The refinement then proceeded normally until all parameter shifts were less than a tenth of the standard deviations at an R value of 0·08 for the reflections used. The function minimized was $\Sigma\omega(F_o-KF_c)^2$ where K is the scale factor. The weighting factor used in the final IBM 7090 calculations were given by $\sqrt{\omega}=1/(\sigma|F_o|)$ where $\sigma=A+B|F_o|+C|F_o|^2)$ and $A=2F_{\text{minimum}}$, $B=1\cdot0$, $C=2/F_{\text{maximum}}$.

The final parameters are given in Table 2. The standard deviations quoted are those computed from the diagonal elements of the normal equations matrix by the least-squares program. When these new parameters are expressed in Å with the use of the Fe_3C lattice dimensions, they show what extraordinarily good values were determined by Lipson & Petch (1940) from their powder analysis*. The greatest change in iron atom positions, although small, is nevertheless thirty times the estimated standard deviation of this analysis, and that of the carbon atoms is ten times the estimated standard deviations. The observed and calculated structure factors are given in Table 3. The Fe atomic scattering factors of Thomas & King, (1962) were modified for the 10% manganese, and complete disorder of the metal atoms was assumed. The small dispersion correction, which was a constant $-0\cdot3$ for $\Delta f'$ over all sin θ ranges, was omitted as negligible.

Description of the structure

The cementite structure has been correctly described as a framework of almost close-packed iron atoms held together by metallic bonding with the small carbon atoms in the largest interstices (Lipson & Petch, 1940). In two recent publications Andrews (1963, 1964) has described the atomic translations necessary to relate the iron atom positions in the structure to those

* A recent analysis using a least-squares procedure (Herbstein & Smits, 1964) on more extensive powder data did not significantly improve on these earlier results.

Table 2. *Atomic parameters of* $(Fe_{2\cdot7}Mn_{0\cdot3})C$ *and* Fe_3C

	$Fe_{2\cdot7}Mn_{0\cdot3}C$					Fe_3C	
						Coordinates	
	Fractional coordinates	σ	Anisotropic temperature factor	σ	Coordinates (Å)	Inferred (this work)	Lipson & Petch
Fe (general)	$x/a=0\cdot1816$	0·0003	$\beta_{11}=0\cdot0010$	0·0005	0·9189	0·924	0·931
	$y/b=0\cdot0666$	0·0001	$\beta_{22}=0\cdot0027$	0·0001	0·4493	0·449	0·438
	$z/c=0\cdot3374$	0·0002	$\beta_{33}=0\cdot0048$	0·0002	1·5208	1·527	1·506
			$\beta_{12}=0\cdot0002$				
			$\beta_{13}=0\cdot0009$				
			$\beta_{23}=0\cdot0000$				
Fe (special)	$x/a=0\cdot0367$	0·0004	$\beta_{11}=0\cdot0027$	0·0008	0·1857	0·187	0·204
	$y/b=0\cdot2500$		$\beta_{22}=0\cdot0026$	0·0001	1·6866	1·686	1·686
	$z/c=0\cdot8402$	0·0002	$\beta_{33}=0\cdot0054$	0·0002	$-0\cdot7203$	$-0\cdot723$	$-0\cdot755$
			$\beta_{13}=0\cdot0001$				
C (special)	$x/a=0\cdot877$	0·003	$\beta_{11}=0\cdot035$	0·005	$-0\cdot622$	$-0\cdot626$	$-0\cdot71$
	$y/b=0\cdot250$		$\beta_{22}=0\cdot005$	0·0006	1·687	1·686	1·686
	$z/c=0\cdot444$	0·002	$\beta_{33}=0\cdot022$	0·002	2·001	2·009	2·13
			$\beta_{13}=-0\cdot004$				

Table 3. *Observed and calculated structure factors*

h	k	l	F_o	F_c	h	k	l	F_o	F_c	h	k	l	F_o	F_c	h	k	l	F_o	F_c	h	k	l	F_o	F_c
0	0	2	84.0	-86.3	1	1	1	12.6	8.6	2	1	1	73.4	88.3	3	3	2	94.6	-109.4	4	8	1	26.4	-26.4
0	0	4	84.7	-83.0	1	1	2	83.9	91.7	2	1	2	38.0	40.9	3	3	3	1.8	-1.6	4	8	4	12.7	-11.5
0	0	6	86.6	84.0	1	1	3	33.3	-33.8	2	1	3	8.3	7.9	3	3	4	75.9	77.4	4	8	5	19.7	21.4
0	0	8	21.3	-18.2	1	1	4	45.0	-39.3	2	1	4	29.8	28.2	3	3	6	14.2	13.2	4	8	6	17.6	16.6
0	0	10	36.7	-33.2	1	1	5	9.4	8.3	2	1	5	48.3	-45.7	3	3	8	47.5	-45.8	4	8	7	13.7	-15.7
0	0	12	26.8	28.2	1	1	6	7.1	-5.8	2	1	5	48.3	-45.7	3	3	10	23.9	24.1	4	9	0	50.2	-47.4
0	1	1	7.7	5.6	1	1	7	10.7	9.1	2	1	6	34.8	-30.8	3	3	12	6.1	8.3	4	9	2	21.1	19.9
0	1	5	12.8	-13.3	1	1	8	28.7	25.6	2	1	7	27.0	23.4	3	4	1	19.2	20.9	4	9	4	24.1	24.0
0	1	7	2.3	-.7	1	1	9	8.0	-8.2	2	2	1	78.8	-91.1	3	4	2	27.2	23.9	4	10	1	33.8	-32.8
0	1	9	2.6	3.0	1	1	10	11.7	-11.8	2	2	2	47.4	46.4	3	4	3	20.8	-19.1	4	10	4	6.8	5.7
0	1	11	2.9	-1.5	1	2	1	54.0	-49.7	2	2	3	13.6	-15.4	3	4	4	25.0	-21.4	4	10	5	23.6	28.4
0	2	0	10.7	7.3	1	2	2	61.9	65.5	2	2	4	47.7	44.9	3	5	1	29.4	-31.2	4	10	7	16.9	-17.7
0	2	2	22.2	-25.8	1	2	3	82.4	86.5	2	2	5	43.0	39.7	3	5	2	33.9	-34.4	4	11	0	24.8	-23.1
0	2	4	7.3	-8.0	1	2	4	34.4	-29.1	2	2	6	51.3	-46.5	3	5	3	38.9	36.7	4	11	1	16.8	-15.5
0	2	8	5.2	-3.2	1	2	5	23.3	-19.0	2	2	7	30.0	-26.5	3	5	4	22.6	20.9	4	12	1	24.3	20.7
0	2	10	3.4	-1.8	1	2	7	30.3	-26.2	2	2	8	7.9	8.0	3	5	5	8.6	-7.9	4	12	5	17.9	-18.6
0	2	12	1.9	4.9	1	2	8	20.8	19.3	2	2	10	19.8	19.1	3	6	1	41.3	-50.2	4	12	7	11.2	11.3
0	3	3	8.8	-3.6	1	2	9	26.4	23.4	2	2	11	19.1	17.2	3	6	3	67.8	71.0	4	13	0	37.1	-35.5
0	3	5	94.1	96.1	1	2	10	10.0	-10.9	2	2	12	14.6	-15.6	3	6	7	28.3	-28.6	4	13	2	16.7	15.2
0	3	7	51.7	-47.2	1	3	1	68.6	81.8	2	3	1	20.1	19.4	3	6	9	33.8	32.2	4	13	4	19.8	18.7
0	3	11	33.1	33.4	1	3	2	13.4	-17.6	2	3	2	22.4	17.0	3	7	1	12.3	13.5	4	13	6	27.6	-25.9
0	4	0	43.9	68.0	1	3	3	90.8	-93.6	2	3	4	22.4	19.9	3	7	2	30.1	-30.5	4	14	1	12.5	11.8
0	4	2	12.7	-7.8	1	3	5	27.4	23.3	2	3	5	11.5	-10.1	3	7	3	14.2	-13.6	4	14	5	10.5	-10.4
0	4	4	20.5	-18.3	1	3	7	31.4	28.3	2	3	6	25.5	-24.9	3	7	4	25.0	25.9	4	15	4	6.0	-5.5
0	4	6	18.9	17.6	1	3	9	38.1	-32.3	2	3	7	9.4	7.3	3	7	8	17.6	-17.2	4	16	1	20.7	23.9
0	4	8	3.6	-3.7	1	4	1	28.2	23.7	2	4	0	46.0	59.3	3	8	1	13.7	-13.2	4	16	5	25.2	-21.6
0	4	10	10.4	-9.2	1	4	3	50.4	-50.5	2	4	1	30.4	31.9	3	8	2	26.1	27.0	5	0	1	25.7	-25.8
0	4	12	1.6	5.8	1	4	4	4.6	-5.9	2	4	2	23.6	-21.7	3	8	3	27.5	30.0	5	0	3	48.1	47.6
0	5	1	35.1	-37.8	1	4	5	10.7	10.9	2	4	3	7.9	10.4	3	8	4	23.0	-23.2	5	0	4	12.7	9.9
0	5	3	5.4	-8.2	1	4	7	21.0	17.9	2	4	4	25.0	-23.6	3	8	5	11.5	-10.8	5	0	7	21.5	-19.0
0	5	5	15.8	14.2	1	4	9	14.6	-14.6	2	4	5	15.0	-12.1	3	8	8	17.4	16.8	5	0	9	19.5	19.8
0	5	7	18.1	-15.3	1	5	1	31.5	27.4	2	4	6	28.3	24.6	3	8	9	15.0	14.5	5	1	1	29.1	-26.8
0	5	9	3.5	-.4	1	5	2	70.7	75.8	2	4	7	12.0	10.1	3	9	2	39.3	39.7	5	1	2	34.6	36.1
0	5	11	8.4	8.7	1	5	3	56.5	-57.0	2	4	8	4.5	-3.7	3	9	4	29.1	-33.4	5	1	3	51.7	48.3
0	6	2	43.2	39.8	1	5	4	44.7	-40.7	2	4	10	10.7	-10.8	3	9	9	4.2	3.2	5	1	4	30.3	-28.7
0	6	4	50.6	48.3	1	5	5	18.9	15.8	2	5	0	64.3	-75.3	3	9	10	12.8	-12.6	5	1	5	14.4	-12.6
0	6	6	59.9	-57.1	1	5	6	5.2	-6.2	2	5	1	69.8	81.3	3	10	1	23.9	-23.0	5	1	7	22.0	-18.8
0	6	8	16.1	13.0	1	5	7	20.2	19.2	2	5	2	38.9	41.6	3	10	3	33.4	34.7	5	1	8	17.6	18.7
0	6	10	26.9	25.0	1	5	8	32.2	29.4	2	5	3	8.1	7.7	3	10	5	9.0	-10.8	5	1	9	20.3	19.0
0	7	1	42.2	-42.2	1	5	9	21.2	-20.1	2	5	4	37.2	34.8	3	10	7	16.4	-16.3	5	2	1	38.4	-36.6
0	7	3	2.8	.9	1	5	10	14.6	-14.5	2	5	5	51.3	-52.8	3	10	9	17.8	18.4	5	2	2	58.1	-57.4
0	7	5	37.9	36.4	1	6	2	56.2	-56.5	2	5	6	47.2	-42.8	3	11	1	17.0	15.0	5	2	3	50.0	51.1
0	7	7	17.4	-17.4	1	6	3	11.2	13.0	2	5	7	32.1	29.7	3	11	2	22.8	20.5	5	2	4	39.9	37.9
0	7	9	7.8	-6.4	1	6	4	47.1	45.7	2	5	11	20.3	-21.6	3	11	3	22.9	-21.2	5	2	5	15.7	-13.4
0	7	11	13.2	13.6	1	6	6	11.2	8.5	2	6	1	26.3	24.1	3	11	4	19.2	-15.4	5	2	7	21.6	-20.6
0	8	0	28.7	-23.0	1	6	7	9.7	-6.7	2	6	5	22.4	-21.7	3	11	8	11.1	12.6	5	2	8	30.1	-27.5
0	8	2	17.8	19.1	1	6	8	29.9	-27.6	2	6	6	4.2	4.6	3	11	9	9.6	-11.3	5	2	10	14.2	14.4
0	8	4	12.9	13.3	1	6	10	14.7	14.6	2	6	7	12.1	11.7	3	12	1	15.8	14.4	5	3	2	41.5	41.8
0	8	6	22.7	-20.6	1	7	1	15.8	17.6	2	7	0	8.8	-3.6	3	12	3	24.3	-21.6	5	3	4	28.8	-26.7
0	8	8	4.6	5.6	1	7	2	27.8	-28.7	2	7	1	18.6	-18.5	3	12	7	9.5	10.7	5	4	1	13.5	14.0
0	8	10	4.3	6.3	1	7	3	17.7	-16.5	2	7	5	15.8	14.2	3	12	9	11.0	-11.8	5	4	2	34.7	31.6
0	9	1	53.9	49.1	1	7	4	13.4	12.8	2	8	0	66.2	67.8	3	13	2	31.2	30.1	5	4	3	16.6	-16.8
0	9	3	3.8	1.2	1	8	1	28.4	25.2	2	8	1	52.1	52.4	3	13	4	26.7	-25.9	5	4	4	23.2	-19.5
0	9	5	45.0	-44.1	1	8	2	43.2	-44.0	2	8	2	28.3	-27.5	3	13	8	21.5	19.9	5	5	1	30.4	-29.9
0	9	7	25.7	24.2	1	8	3	50.0	-50.8	2	8	4	31.8	-32.5	3	14	7	4.4	5.6	5	5	2	47.6	50.5
0	9	9	6.9	7.9	1	8	4	29.6	28.3	2	8	5	37.8	-35.8	3	15	2	5.7	-7.9	5	5	3	54.4	54.6
0	9	11	17.1	-18.6	1	8	5	14.8	14.4	2	8	6	42.7	40.6	3	15	4	7.6	7.0	5	5	4	41.5	-40.2
0	10	0	54.4	-54.8	1	8	7	23.1	22.0	2	8	7	25.5	25.7	3	16	1	15.7	15.5	5	5	5	16.4	-16.4
0	10	2	19.4	17.0	1	8	8	23.4	-22.8	2	8	8	12.1	-7.8	3	16	3	23.0	-25.9	5	5	7	25.0	-22.4
0	10	4	25.1	24.3	1	8	9	21.9	-21.6	2	8	10	18.2	-18.3	4	0	1	93.3	123.8	5	5	8	29.1	29.1
0	10	6	31.5	-31.6	1	8	10	12.3	12.9	2	8	11	16.8	-17.7	4	0	3	9.5	11.4	5	5	9	24.3	24.6
0	10	8	6.3	7.4	1	9	1	22.2	-22.6	2	9	0	17.7	17.0	4	0	4	10.3	-9.4	5	5	10	12.3	-14.5
0	10	10	14.8	14.9	1	9	2	13.3	14.7	2	11	0	44.9	37.1	4	0	5	78.1	-76.8	5	6	1	11.0	13.2
0	11	1	22.4	19.1	1	9	3	30.5	29.8	2	11	1	40.7	-38.6	4	0	7	46.6	44.2	5	6	3	27.2	-27.0
0	11	3	3.2	3.4	1	9	5	10.0	-9.1	2	11	2	21.2	-20.2	4	0	9	13.4	12.3	5	8	1	29.3	28.7
0	11	5	12.4	-12.4	1	9	7	11.6	-13.1	2	11	4	19.9	-20.9	4	0	11	26.2	-31.6	5	8	3	41.6	-45.5
0	11	7	12.5	12.1	1	9	8	6.7	7.0	2	11	5	32.9	33.8	4	1	1	32.9	33.9	5	8	4	31.3	-32.5
0	11	9	1.5	.9	1	9	9	16.7	15.7	2	11	6	30.4	29.4	4	1	3	8.2	7.6	5	8	5	13.0	13.4
0	12	0	36.9	34.6	1	10	2	22.7	-21.5	2	11	7	20.8	-21.0	4	1	5	16.6	-16.1	5	8	7	18.4	21.4
0	12	2	10.4	-10.4	1	10	3	13.1	13.2	2	12	0	9.8	9.3	4	1	7	12.1	12.1	5	8	8	25.9	25.7
0	12	4	17.9	-16.1	1	10	4	20.1	20.5	2	12	4	6.7	-5.3	4	2	0	26.9	-32.3	5	8	9	23.1	-23.6
0	12	6	21.8	20.8	1	10	8	14.1	-14.0	2	12	6	4.6	6.0	4	2	1	23.0	23.0	5	8	10	12.5	-14.2
0	12	8	4.9	-4.5	1	11	1	16.6	-14.5	2	12	8	2.7	-.5	4	2	2	21.5	21.5	5	9	2	13.2	-12.9
0	13	1	40.4	34.5	1	11	2	36.3	-35.0	2	13	0	13.9	13.8	4	2	4	18.2	16.2	5	9	8	7.8	-7.7
0	13	3	3.1	1.6	1	11	3	30.7	31.5	2	14	0	34.8	-31.0	4	2	5	12.7	-14.4	5	11	1	19.7	18.1
0	13	5	32.2	-33.2	1	11	4	24.5	23.9	2	14	1	22.4	-23.3	4	2	6	22.3	-20.3	5	11	2	32.6	-32.7
0	13	7	21.1	19.7	1	11	5	11.9	-10.5	2	14	2	14.3	13.0	4	3	1	13.2	-14.2	5	11	3	36.6	-34.5
0	13	9	4.5	6.0	1	11	7	13.7	-14.3	2	14	4	17.6	16.7	4	3	2	50.0	-50.1	5	11	4	26.4	27.4
0	14	0	11.2	9.1	1	11	8	21.2	-20.7	2	14	5	19.8	18.9	4	3	4	55.1	-51.8	5	11	5	10.7	11.4
0	14	2	6.8	-7.3	1	11	9	16.1	15.8	2	14	6	22.8	-22.2	4	3	6	67.6	63.4	5	11	8	21.5	-21.8
0	14	4	4.5	-5.6	1	11	10	9.9	10.5	2	16	1	9.7	-8.5	4	3	10	25.3	-26.4	5	11	9	18.3	-17.9
0	14	6	10.5	9.5	1	12	3	13.6	-13.7	2	17	2	6.0	7.5	4	4	0	18.6	19.4	5	12	2	11.8	9.6
0	14	8	1.0	-2.9	1	12	4	14.5	-11.7	2	18	0	9.3	-11.3	4	4	1	20.8	20.6	5	13	2	13.0	-11.3
0	15	1	10.0	-10.5	1	13	1	16.2	-15.6	2	18	1	4.9	-7.2	4	4	2	15.7	-14.5	5	13	4	9.1	8.2
0	15	3	2.7	.2	1	13	3	25.7	23.5	3	0	1	78.4	97.6	4	4	5	17.6	-14.4	5	14	1	14.9	-14.4
0	15	5	12.8	11.4	1	13	7	11.2	-11.1	3	0	2	4.1	-1.8	4	4	6	16.3	14.4	5	14	2	24.6	-22.1
0	15	7	1.9	-5.5	1	13	9	13.1	13.3	3	0	3	115.8	-124.2	4	5	0	32.0	36.6	5	14	3	24.8	23.9
0	16	0	40.4	34.7	1	14	1	13.8	-12.0	3	0	5	33.6	31.7	4	5	1	28.5	29.7	5	14	4	18.3	17.4
0	16	2	10.1	-13.0	1	14	2	18.3	19.0	3	0	6	2.3	-2.0	4	5	2	15.7	-15.8	5	14	5	8.0	-7.2
0	16	4	21.1	-17.3	1	14	3	19.1	24.5	3	0	7	40.0	39.7	4	5	4	15.5	-15.0	5	14	7	11.1	-11.9
0	16	6	28.1	23.7	1	14	4	13.8	-13.9	3	0	9	48.6	-43.8	4	5	5	18.1	-17.0	5	15	3	11.5	-10.9
0	17	1	5.1	-4.1	1	14	7	12.1	-12.2	3	1	1	34.9	-37.3	4	5	6	21.5	20.8	5	16	3	8.1	11.0
0	17	3	1.3	-.8	1	14	8	11.3	12.0	3	1	3	40.6	37.2	4	6	1	62.7	-68.9					
0	17	5	.9	2.3	1	15	2	9.5	-12.5	3	1	5	5.5	-7.1	4	6	5	53.6	52.3					
0	18	0	8.6	-4.8	1	16	2	18.0	18.1	3	1	7	12.2	-12.9	4	6	7	35.4	-31.8					
0	18	2	1.5	.5	1	16	4	14.7	-16.1	3	1	9	16.0	13.5	4	6	11	19.1	23.5					
1	0	1	5.1	-6.3	2	0	1	77.2	-63.6	3	2	1	9.9	8.1	4	7	0	37.3	36.5					
1	0	2	109.4	124.8	2	0	2	16.9	13.5	3	2	2	45.9	-42.7	4	7	1	15.1	-14.3					
1	0	3	10.5	-11.8	2	0	4	9.4	9.0	3	2	3	27.7	-27.1	4	7	2	15.9	-14.9					
1	0	4	83.5	-81.6	2	0	5	38.2	39.1	3	2	4	36.1	32.9	4	7	4	19.1	-17.7					
1	0	6	12.9	-12.7	2	0	6	14.0	-12.9	3	2	7	9.6	7.2	4	7	6	24.5	22.8					
1	0	8	44.2	39.5	2	0	7	21.2	-19.6	3	2	8	19.9	-18.5	4	7	10	8.7	-10.3					
1	0	10	22.6	-20.7	2	0	11	10.9	12.7	3	3	1	8.7	10.1	4	8	0	22.0	20.5					

OMITTED FROM REFINEMENT

0	3	1	114.3	-167.2
0	6	0	93.0	-116.5
2	1	0	53.0	-70.0
2	2	0	73.0	-123.9
2	3	0	51.3	-73.3
4	3	0	104.2	120.2

in α-iron and ε-Fe_3C. In particular, Andrews points out that by small atomic shifts it is possible to transform a close-packed cubic [111] row of iron atoms into the zigzag rows which occur in the cementite structure. He also relates these rows to the hexagonal iron lattice in the ε-carbide.

In cubic close-packed iron, (γ–Fe), the volume per atom is 11·47 Å^3, and in the body-centered structure (α–Fe), it is about 3% greater. The corresponding free volume per iron atom in Fe_3C is 12·94 Å^3. This is 12% greater than the close-packing volume, so clearly a purely interstitial description of the role for the carbon atoms in Fe_3C is an over-simplification. The iron lattice in the cementite structure differs from that of a close-packed structure by reason of the necessity to accommodate carbon atoms in the ratio of 1:3. From this point of view, the arrangement of the iron atoms of the cementite structure is best described by starting with the hexagonal close-packed structure, type *A*3, which is a hypothetical structure of the metal but is the ε-phase for the alloy with 10 to 30% manganese. This structure is then compressed in a $[10\bar{1}0]$ direction so that the basal hexagonal layers fold at the lines of intersection of the $(2\bar{1}\bar{1}0)$ planes to form regularly pleated-layers as shown in Figs. 1 and 2. The folding is alternately up and down and is symmetrical, so that the $(2\bar{1}\bar{1}0)$ planes retain their mirror symmetry property, as illustrated in Fig. 2. They bisect the folding angle of 112·2°. The $[a]_H$, $[21\bar{3}0]_H$, $[c]_H$ axes of the original hexagonal structure then become the [*b*], [*c*], and [*a*] axes respectively in the cementite structure. The $(2\bar{1}\bar{1}0)$ mirror planes in the h.c.p. structure become the mirror planes at $y=\frac{1}{4}, \frac{3}{4}$ in the space group *Pnma*. The iron atoms which lie in these planes, *i.e.* on the fold-lines, are those in the 4-fold (*c*) positions. The characteristic *ABAB* close-packed hexagonal arrangement of successive layers in the $[c]_H$ direction of the *A*3 structure is maintained along the [*a*] direction of the cementite structure, so that the atoms of one pleated layer lie over the interstices of those in the layer below.

At the line of intersection of the mirror planes and the pleated layers, *i.e.* on the fold-lines, the iron atoms are separated by two sets of interstices, *X* and *Y* in Fig. 3. The carbon atoms occupy these *X*, *Y* sites in an ordered manner, alternating at *X* and *Y* between successive pleated-layers. There are theoretically possible two other carbon atom arrangements making use of

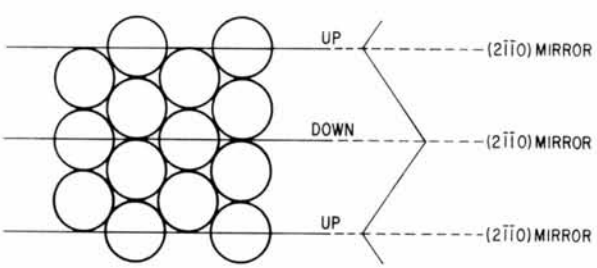

Fig. 1. Forming of regularly pleated layers.

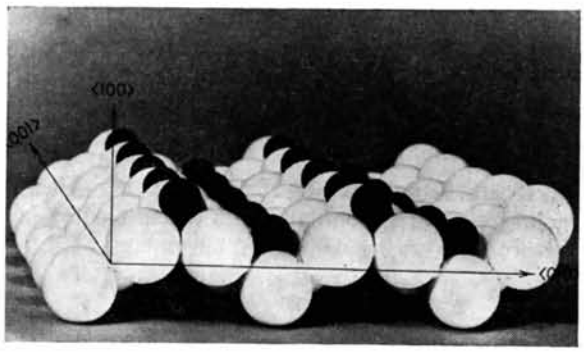

Fig. 2. Regular pleated layer of the cementite structure.

these 4-fold [*c*] type interstices and consistent with the Fe_3C stoichiometry. These are (1), *X* and *Y* sites both occupied and both vacant between alternate layers, and (2), all *X* sites (or all *Y* sites) occupied between successive layers. The actual arrangement is that in which the adjacent carbon atoms are furthest apart, as shown in Fig. 3.

The relationship between this pleated-layer structure of the Fe atoms and the h.c.p. arrangement from which it can be derived is defined by a single parameter, the fold-angle at the $(11\bar{2}0)$ mirror planes. With the fold-angle observed in the cementite structure we can therefore deduce the parameters of the corresponding most close-packed pleated-layer iron structure.

Assuming the metallic radius of the c.c.p. structure of γ–Fe, the hypothetical h.c.p. structure, *i.e.* pure ε-iron, has calculated lattice dimensions $a=2{\cdot}532$, $c=4{\cdot}135$ Å. In the corresponding ε-phase the following

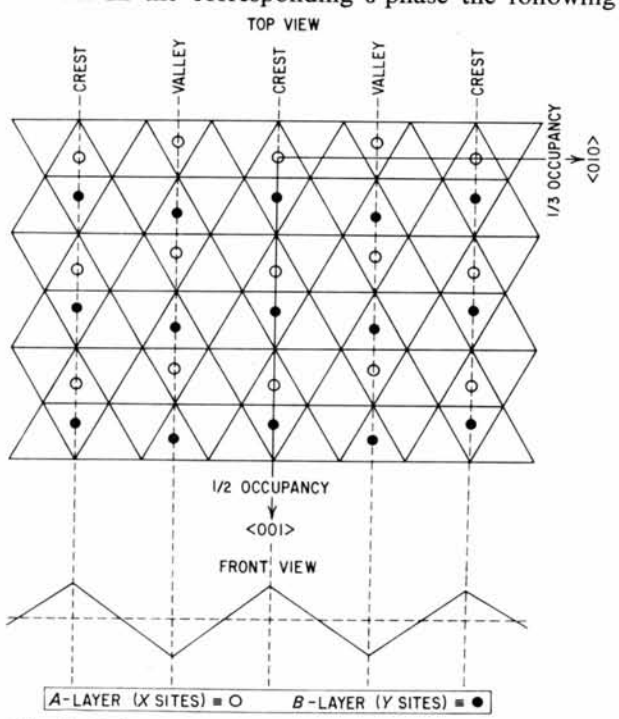

Fig. 3. Carbon atom positions on *A* and *B* pleated layers.

values have been reported (Pearson, 1958), again indicating a contraction of the lattice on the introduction of less than 20% manganese:

18·5% manganese $a=2{\cdot}530$, $c=4{\cdot}079$ Å
22·9% manganese $a=2{\cdot}546$, $c=4{\cdot}114$ Å

With the fold-angle of 112·2° found in this cementite structure, the corresponding hypothetical pleated-layer structure for iron has calculated parameters:

$a=4{\cdot}722$, $b=6{\cdot}736$, $c=4{\cdot}385$ Å.
Fe (general positions)
$x/a=0{\cdot}191$ $y/b=0{\cdot}062$ $z/c=0{\cdot}395$
Fe (special positions)
$x/a=0{\cdot}010$ $y/b=\frac{1}{4}$ $z/c=-0{\cdot}104$

This is, in fact, no longer a close-packed structure, since the pleated layers do not fit as compactly as plane layers. The volume per iron atom is 1·3% greater and this corresponds, of course, to increased space available between the metal atoms at the interstitial sites.

The actual cementite structure has a further increase in the lattice dimensions, as seen by comparing the data in Table 1 with those derived above. This increase is principally in the *a*-axis direction, which would be expected since the cementite structure is generated by stacking the pleated layers in this direction with the carbon atoms between the layers. The difference in the iron positional parameters are also such as can be accounted for, at least qualitatively, as distortions of less than 0·3 Å, necessary to make more space available to the carbon atoms. These distortions are also a measure, of course, of the degree to which the pleated-layer description is a rationalization of the actual detailed structure. The iron atoms are not completely planar in each segment of the pleated layer as shown in Fig. 2, but are displaced from the mean plane by ±0·08 Å.

Starting with a h.c.p. array of iron atoms, there is therefore a 1·3% increase in lattice volume when the pleating is introduced, and a further 11·5% increase in volume when the carbon atoms are inserted. It is interesting to compare this expansion of the iron lattice for the cementite structure with that involved in the formation of ε-Fe_3C, which is hexagonal with an *A*3 type iron lattice. The mean volume per iron atom in ε-Fe_3C is 14·0 Å^3, which is a 22% increase over that of close-packing. This is significantly greater than the 13% expansion over close-packing which occurs in the formation of the cementite structure. The explanation for this is that the pleated-layer arrangement of the metal atoms leads to the expansion of certain of the interstices only, *i.e.* those at the ridges of the pleats where the carbon atoms are located; whereas in the *A*3 type iron lattice, all the interstices are expanded by the increase in lattice dimensions, although only one sixth of them are actually occupied by the carbon atoms. Thus one would expect the ε-carbide structure to be normally metastable with respect to the cementite structure, although both structures are in fact observed.

The pleated-layer iron lattice alone would be unstable relative to the corresponding h.c.p. lattice, not only with respect to the small expansion discussed above, but also because the average first-neighbour coordination is less ($11\frac{1}{3}$ *versus* 12). Therefore it is expected that the pleated-layer lattice will be stabilized only by those interstitial atoms which are sufficiently large to render the h.c.p. type lattice unstable relative to the pleated layer, by reason of the preferential expansion of the special interstices. Thus, in the series nitride, carbide, boride, the increase in size of the non-metallic atoms corresponds with an observed trend from the Fe_3N, which has only the ε-structure, through Fe_3C with both ε- and cementite to $Fe_3(B_{0{\cdot}8}C_{0{\cdot}2})$ with only the cementite-type structure.

The interatomic distances

The first-neighbour distances are given in Table 4 and Figs. 4, 5 and 6, calculated from the fractional coordinates with both the $(Fe_{2{\cdot}7}Mn_{0{\cdot}3})C$ and the Fe_3C lattice dimensions. The difference in the lattices result in differences in interatomic distances ranging from insignificant to 0·015 Å. There are no systematic aspects of these differences, and this comparison indicates the limit to which the discussion of the details of the

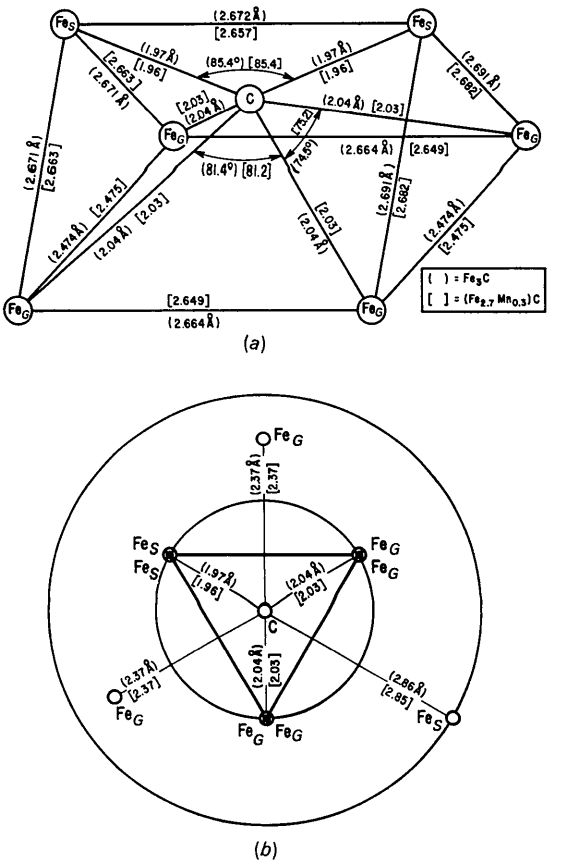

Fig. 4. (*a*) Bond distances of triangular prism enclosing C atom. (*b*) Stereogram of C nearest and next nearest Fe neighbors.

$(Fe_{2\cdot7}Mn_{0\cdot3})C$ structure can be extrapolated to Fe_3C itself. A more precise description of Fe_3C must await the preparation of suitable single crystals.

The intermetallic distances in the $(Fe_{2\cdot7}Mn_{0\cdot3})C$ structure range from 2·475 to 2·682 Å, *i.e.* from values equal to that in α-iron to 10% greater. The atoms in general positions have eleven metal atom neighbours, and those in the special positions have twelve. The stereograms of the coordinations are shown in Figs. 5 and 6. It will be observed that the stereogram of the general metal position shows a marked resemblance to that of h.c.p., with one carbon atom completing the

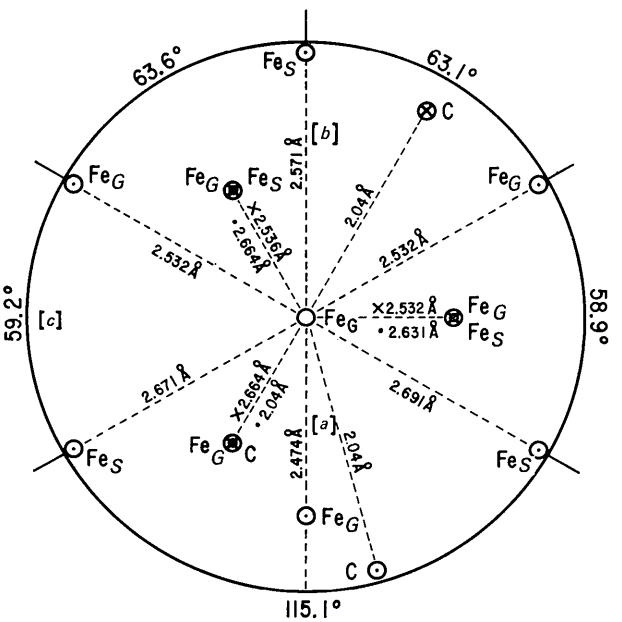

Fig. 5. General position Fe stereogram of Fe_3C.

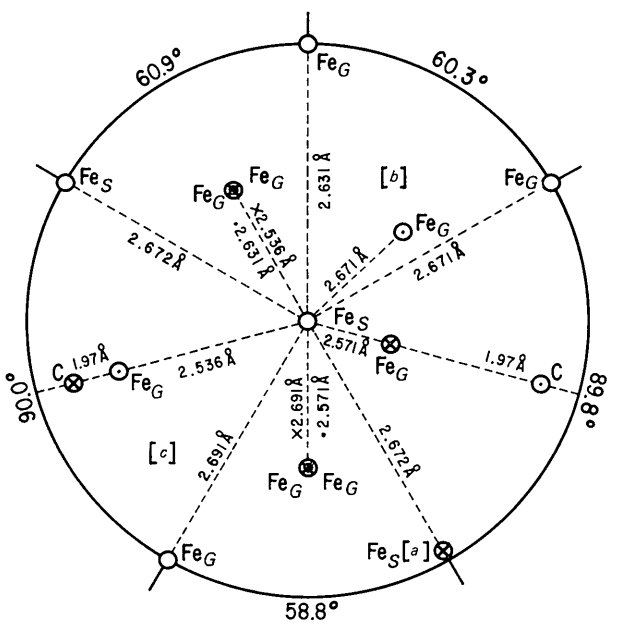

Fig. 6. Special position Fe stereogram of Fe_3C.

Table 4. *Interatomic distances*

Atom notation	Symmetry code		
I	x	y	z
II	$0{\cdot}5+x$	$0{\cdot}5-y$	$0{\cdot}5-z$
III	$-x$	$0{\cdot}5+y$	$-z$
IV	$0{\cdot}5-x$	$-y$	$0{\cdot}5+z$
V	$-x$	$-y$	$-z$
VI	$0{\cdot}5-x$	$0{\cdot}5+y$	$0{\cdot}5+z$
VII	x	$0{\cdot}5-y$	z
VIII	$0{\cdot}5+x$	y	$0{\cdot}5-z$

$Fe_G \equiv$ general position Fe; $Fe_S \equiv$ special position Fe.

Fe–C	$(Fe_{2\cdot7}Mn_{0\cdot3})C$	Fe_3C
Fe_G(I)–C(I)(VII)	2·04 Å	2·04 Å
Fe_G(I)–C(II)(VIII)	2·03	2·04
Fe_S(I)–C(I)	1·96	1·97
Fe_S(I)–C(II)	1·97	1·98
Fe_G–$Fe_{G,S}$		
Fe_G(I)–Fe_G(VII)	2·475	2·474
Fe_G(I)–Fe_G(V)	2·517	2·532
Fe_G(I)–Fe_G(IV, IV)	(2) 2·523	(2) 2·532
Fe_G(I)–Fe_S(III)	2·534	2·536
Fe_G(I)–Fe_S(VI)	2·568	2·571
Fe_G(I)–Fe_S(II)	2·621	2·631
Fe_G(I)–Fe_G(VIII, VIII)	(2) 2·649	(2) 2·664
Fe_G(I)–Fe_S(I)	2·663	2·671
Fe_G(I)–Fe_S(VII)	2·682	2·691
Fe_S–$Fe_{G\cdot S}$		
Fe_S(I)–Fe_G(III, V)	(2) 2·534	(2) 2·536
Fe_S(I)–Fe_G(IV, VI)	(2) 2·568	(2) 2·571
Fe_S(I)–Fe_G(II, VII)	(2) 2·621	(2) 2·631
Fe_S(I)–Fe_G(I, VII)	(2) 2·663	(2) 2·671
Fe_S(I)–Fe_S(II, II)	(2) 2·657	(2) 2·672
Fe_S(I)–Fe_G(I, VII)	(2) 2·684	(2) 2·693

12-coordination, and two additional carbon atoms near the equatorial plane. The stereogram of the atom in the special position is much more irregular, and shows no such similarity, as would be expected since these atoms are on the ridges of the pleated layers. There is a small but significant systematic difference in the distribution of the intermetallic distances. For $Fe(Mn)_G - Fe(Mn)_G$, the distances range from 2·475 to 2·649 with a mean value of 2·555 Å. For $Fe(Mn)_G - Fe(Mn)_S$, the range is 2·534 to 2·682 with a mean of 2·613 Å, and for $Fe(Mn)_S - Fe(Mn)_S$ the distance is 2·657 Å. Thus the twelve coordinated iron atoms in the special positions have a significantly greater mean radius, by 0·05 Å, than the eleven coordinated atoms. This is consistent with the generally observed increase in atomic radius with coordination number.

The carbon atom coordination is 6-fold in a triangular prism as described by Lipson & Petch (1940) and illustrated in Fig. 4. The four independent Fe(Mn)–C distances fall into two groups; $Fe(Mn)_S$–C with mean value of 1·968 Å and $Fe(Mn)_G$–C with mean value of 2·032 Å. This difference of 0·06 Å is at the 99·0 significance level by the Cruickshank (1940) criterion. It is comparable in magnitude to the difference in the metallic radii discussed above, but in the reverse sense. The Fe(Mn)–C distance associated with the metal atoms in the general eleven-coordinated positions is the longer. Clearly any argument based on the addition of atomic

radii of spherical atoms cannot account for both the metal to metal and metal to carbon distances, and the difference in the two metal—carbon distances cannot thereby be simply interpreted in terms of a preferential ordering of the Mn atoms in special or general positions. However, it is interesting to note that these interatomic distances are universely related to the first neighbour coordination number if we consider the metal to metal and metal to nonmetal bonding *separately*. Thus Fe_S has 12 Fe and 2 C, Fe_G has 11 Fe and 3 C, $Fe_S-Fe_S > Fe_S-Fe_G > Fe_G-Fe_G$ and $Fe_G-C > Fe_S-C$, (see Figs. 5 and 6).

The values and orientation of the principal axes of the atomic thermal vibration ellipsoids are given in Table 5 and Fig. 8. They show that the two types of iron atom are very similar in their thermal behavior. The ellipsoids have a nearly circular cross section in the (100) plane and the axis of minimum vibration inclined at about 10° to [100]. The carbon atoms are more anisotropic, having their maximum principal axis also about 10° to [100], in the direction of the axis of the trigonal prism, shown in Fig. 4.

These thermal parameters describe the shape of the atomic electron-density distributions and, irrespective of whether the anisotropy is due to the time-average effect of thermal motion or the space-average effect of disorder caused by the 10% Mn atoms, they should be related in at least a qualitative measure to the 'tightness' of the packing of the atoms. Nicholson (1954) found that when the carbon in cementite is substituted by boron the lattice parameter changed anisotropically as shown in Fig. 7. Since boron is generally considered to be slightly larger than carbon, it is consistent that the direction of maximum expansion, [*a*], is the direction of tightest fit and minimum thermal spread of the iron electron density in the structure. On the other hand, the contractions in the [*b*] and [*c*] axial directions suggest that this substitution is also accompanied by a subtle change in the nature of the metal–nonmetal bonding.

Table 5. *The thermal ellipsoids*

R.M.S. displacements in Å, and directions of principal axes in degrees (calculated from parameters in Table 2 with IBM 1620 program by Shiono, 1964)

	i	$\lvert r_i^2\rvert^{\frac{1}{2}}$	g_{ia}	g_{ib}	g_{ic}
	1	0·080	83·6	10·0	82·4
Fe_G	2	0·072	104·7	80·9	162·6
	3	0·032	16·0	94·2	105·5
	1	0·077	90	0	90
Fe_S	2	0·075	94·1	90	175·8
	3	0·059	4·1	90	94·1
	1	0·216	11·1	90	101·1
C	2	0·149	101·1	90	168·9
	3	0·110	90	0	90

We wish to thank Mr L. Zwell, Mr J. C. Raley, Dr R. M. Fisher and Mr A. Szirmae for advice and for assistance in preparation of the crystals, Mr J. Gula for the microprobe analysis, and Dr G. Dutta and Mr R. Whitmore for assistance with the computations.

This work was supported, in part, by the U.S. Army Research Office, Durham, through Grant ARO(D)-31-124-G412.

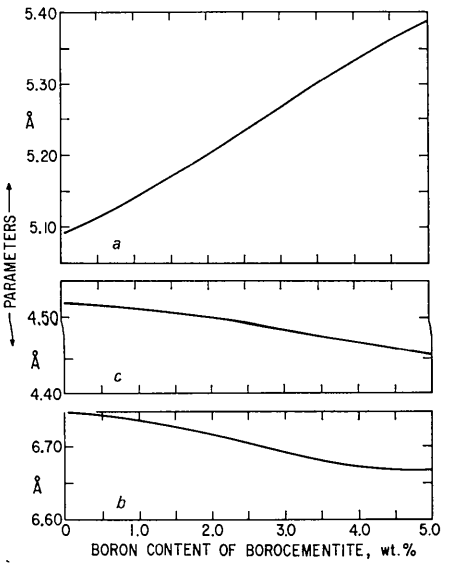

Fig. 7. Lattice parameters of borocementite.

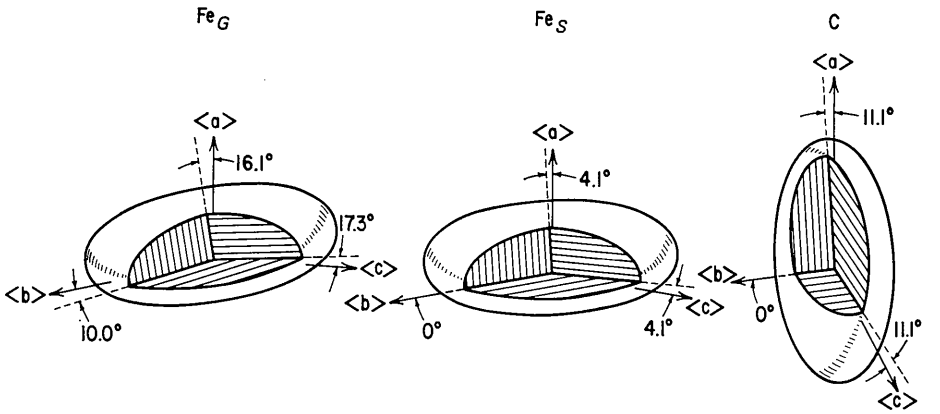

Fig. 8. Atomic thermal ellipsoids of $Fe_{2\cdot7}Mn_{0\cdot3}C$.

References

ANDREWS, K. W. (1963). *Acta Metallurg.* **11**, 939.
ANDREWS, K. W. (1964). *Acta Metallurg.* **12**, 921.
ARONSSON, B. & RUNDQUIST, S. (1962). *Acta Cryst.* **15**, 878.
BUSING, W. R., MARTIN, K. O. & LEVY, H. A. (1962). *ORFLS Fortran Crystallographic Least Squares Program.* ORNL-TM-305.
CARPENTER, G. B. (1963). *Computer Programs of Brown University* III, *C* 2, 1.
CRUICKSHANK, D. W. J. (1949). *Acta Cryst.* **2**, 65.
CRAVEN, B. (1963). *Univ. Pittsburgh Crystallographic Computing Programs, Tech. Rep.* **42**, 1.
DAUBEN, C. H. & TEMPLETON, D. H. (1955). *Acta Cryst.* **8**, 841.
DUTTA, S. N. (1964). Private communication.
GARDIN, A. I. (1962). *Soviet Phys. Crystallogr.* **7**, 854.
HENDRICKS, S. B. (1930). *Z. Kristallogr.* **74**, 534.
HERBSTEIN, F. H. & SMUTS, J. (1964). *Acta Cryst.* **17**, 1331.
International Tables for X-ray Crystallography (1959). Vol. II. Birmingham: Kynoch Press.
KUO, K. & PERSSON, K. & PERSSON, L. E. (1954). *J. Iron Steel Inst.* **178**, 39.
LIPSON, H. & PETCH, N. J. (1940). *J. Iron Steel Inst.* **142**, 95.
LYASHCHENKO, B. G. & SOROKIN, L. M. (1963). *Soviet Phys. Crystallogr.* **8**, No. 3.
MEINHARDT, D. & KRISEMENT, O. (1962). *Arch. Eisenhüttenw.* **7**, 493.
NICHOLSON, M. E. (1957). *Trans. Amer. Inst. Min. (metall) Engrs,* **209**, 1.
PEARSON, W. B. (1958). *Lattice Spacings and Structures of Metal Alloys,* p. 630. New York: Pergamon Press.
SHIGETAKA, S. J. (1930). J. *Faculty of Engineering, Tokyo Imperial Univ. XX*, No. 1.
SHIONO, R. (1963). *Univ. Pittsburgh Crystallographic Computing Programs, Tech. Rep.* **43**, 1.
THOMAS, L. H., UMEDA, K. & KING, K. (1962). In *International Tables for X-ray Crystallography.* Vol. III, 210. Birmingham: Kynoch Press.

Short Communications

Contributions intended for publication under this heading should be expressly so marked; they should not exceed about 1000 *words; they should be forwarded in the usual way to the appropriate Co-editor; they will be published as speedily as possible. Publication will be quicker if the contributions are without illustrations.*

Acta Cryst. (1965). **19**, 471

Pseudo-orthorhombic diffraction patterns and OD structures.

By K. DORNBERGER-SCHIFF, *Institut für Strukturforschung der Deutschen Akademie der Wissenschaften zu Berlin, Germany,* and J. D. DUNITZ, *Organic Chemistry Laboratory, Swiss Federal Institute of Technology, Zürich, Switzerland*

(*Received* 16 *February* 1965)

In a recent publication (Dunitz, 1964) the interpretation of certain pseudo-orthorhombic diffraction patterns was discussed in terms of the twinning of monoclinic structures. We wish to point out here that all the pseudo-orthorhombic patterns discussed in the previous paper can equally well, and perhaps more convincingly, be interpreted in terms of OD (order–disorder) structures (Dornberger-Schiff, 1956, 1964; Dornberger-Schiff & Grell-Niemann, 1961), *i.e.* structures consisting of layers such that pairs of successive layers can be formed in two or more geometrically, and hence energetically, equivalent ways. In some cases the previous conclusions are little altered, except that the twinning is to be understood as OD twinning, but for the cycloundecylamine hydrobromide and cobalt dipyridine dichloride cases the previous interpretations may have to be more radically revised.

Para-orthorhombic structures (monoclinic structures in which the projections down three mutually perpendicular directions have perfect rectangular symmetry) are seen to arise naturally from certain types of OD arrangements. This is illustrated by the example, one of many possible, shown in Fig. 1 left. The example shows an ordered arrangement of layers [symmetry P(2)*mb*] in which the relationship between any pair of successive layers is identical and can be described in terms of a displacement by the stacking vector $\mathbf{s}_1 = \mathbf{a}_0 + \mathbf{b}/4$. This ordered arrangement is para-orthorhombic, space group $P11b$ (No. 7, C_s^2); because all triples and higher *n*-tuples of successive layers are geometrically equivalent, such an arrangement is described as having 'maximum degree of order'. We shall refer to it as the arrangement MDO_1. Displacement of any layer by $b/2$, corresponding to the occurrence of a stacking vector $\mathbf{s}_2 = \mathbf{a}_0 - \mathbf{b}/4$, gives an interlayer relationship that is geometrically, and hence energetically, equivalent to that in the ordered arrangement. An arrangement containing long sequences of stacking vectors $\mathbf{s}_1$ alternating with long sequences of vectors $\mathbf{s}_2$ would be an OD twin. For shorter sequences we would speak of polysynthetic twinning or – if the ordered

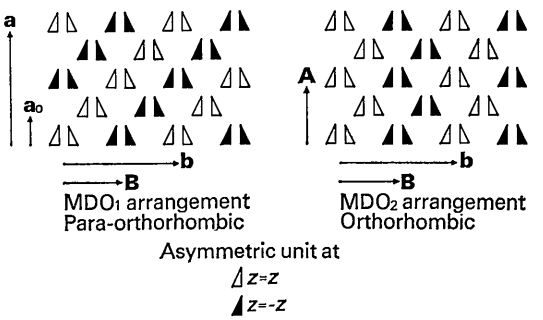

Fig. 1. Schematic representation of two ordered OD-arrangements, MDO_1 and MDO_2, based on the same layers and pairs of layers; **a**, **b**, **c** non-primitive (fourfold) rectangular unit cell of MDO_1 **A**, **B**, **c** unit cell of superposition structure **c** perpendicular to plane of paper.